

# Low-temperature phases in $\text{PbZr}_{0.52}\text{Ti}_{0.48}\text{O}_3$ : A neutron powder diffraction study

D. E. Cox, B. Noheda,\* and G. Shirane

Physics Department, Brookhaven National Laboratory, Upton, NY 11973, USA

(Dated: July 21, 2004)

A neutron powder diffraction study has been carried out on  $\text{PbZr}_{0.52}\text{Ti}_{0.48}\text{O}_3$  in order to resolve an ongoing controversy about the nature of the low-temperature structure of this strongly-piezoelectric and technologically-important material. The results of a detailed and systematic Rietveld analysis at 20 K are consistent with the coexistence of two monoclinic phases having space groups  $Cm$  and  $Ic$  respectively, in the approximate ratio 4:1, and thus support the findings of a recent electron diffraction study by Noheda *et al.* [Phys. Rev. B **66**, 060103 (2002)]. The results are compared to those of two recent conflicting neutron powder diffraction studies of materials of the same nominal composition by Hatch *et al.* [Phys. Rev. B **65**, 212101 (2002)] and Frantti *et al.* [Phys. Rev. B **66**, 064108 (2002)].

PACS numbers: 61.12.Ld, 61.50.Ks, 61.66.Fn, 77.84.Bw

## I. INTRODUCTION

The strongly piezoelectric system  $\text{PbZr}_{1-x}\text{Ti}_x\text{O}_3$  (PZT) has long been known to have a perovskite-type structure with regions of rhombohedral and tetragonal symmetry below the ferroelectric Curie point separated by an almost vertical line at  $x \approx 0.5$  in the temperature-composition phase diagram, which is known as the morphotropic phase boundary (MPB).<sup>1</sup> Following the recent discovery of a narrow region with monoclinic  $Cm$  symmetry in the vicinity of the MPB,<sup>2</sup> numerous experimental and theoretical studies of PZT and related systems have been undertaken in order to clarify the relationships between the structural features and the piezoelectric properties. As previously discussed,<sup>3</sup> the ferroelectric polarization in the new phase is no longer constrained by symmetry to lie along a symmetry axis, but instead is free to rotate within the symmetry plane. Furthermore, because of the near-degeneracy of the free energies of the various phases, rotation of the polarization axis away from the polar axes of the rhombohedral and tetragonal phases can be accomplished with an applied electric field, resulting in an induced monoclinic phase and a large electromechanical response.<sup>4,5</sup>

The phase diagram of the PZT system around the MPB as reported in a recent paper by Noheda *et al.*<sup>6</sup> is shown in Fig. 1. Above the Curie temperature, the structure is cubic over the entire range of composition, with space group  $Pm\bar{3}m$  and lattice parameter  $a_0 \approx 4$  Å. The rhombohedral region is characterized by high- and low-temperature phases ( $R_{HT}$  and  $R_{LT}$ ) in which there are polar shifts of the atoms along the pseudocubic  $[111]$  axis.<sup>7,8</sup>  $R_{HT}$  has space group symmetry  $R\bar{3}m$ , with lattice parameters  $a_R \approx a_0$ , and  $\alpha$  slightly less than  $90^\circ$  (hexagonal values  $a_H \approx a_0\sqrt{2}$ ,  $c_H \approx a_0\sqrt{3}$ ). In  $R_{LT}$  there are additional displacements of the oxygen atoms superimposed on the ferroelectric shifts due to antiphase tilting of the oxygen octahedra about the  $[111]$  axis, corresponding to an R-point instability. As a consequence, the unit cell is doubled and the mirror plane is destroyed, resulting in the appearance of super-

lattice peaks in the diffraction pattern. The new space group symmetry is  $R3c$ , with hexagonal lattice parameters  $a_H \approx a_0\sqrt{2}$  and  $c_H \approx 2a_0\sqrt{3}$ . It should be emphasized that these must be regarded as “average” long-range structures, since the presence of short-range order due to local displacements has been clearly demonstrated by the appearance of other types of superlattice peaks in electron diffraction studies<sup>9,10,11</sup> not observed in x-ray or neutron diffraction patterns.<sup>7,8</sup> Significant deviations of the local atomic structure from the crystallographic long-range structure have also been found from pair-distribution function (PDF) analysis of time-of-flight neutron data.<sup>12,13,14</sup>

In the tetragonal region of the phase diagram, the space group is  $P4mm$  and the polar shifts lie along the  $[001]$  axis ( $a_T \approx c_T \approx a_0$ ,  $c_T/a_T > 1$ ). Nevertheless, the time-of-flight neutron data show that this too should be viewed as an “average” long-range structure. In addition, Raman scattering studies have revealed the presence of local displacements of lower symmetry, which are also reflected in a broadening of some of the x-ray diffraction peaks.<sup>15,16</sup> The nature of the local structure has been revealed in more detail from the PDF analysis described in Ref. 14, which shows that there are only gradual changes through the MPB, and suggests that the local environment of each element remains relatively invariant of composition. It is furthermore proposed that the population of local Pb displacements changes between the pseudocubic  $\langle 100 \rangle$  and  $\langle 110 \rangle$  directions as a function of the Ti/Zr ratio. This model is supported by recent theoretical calculations in which the Pb distortions are identified as the determining factor for the average structure of the system.<sup>17</sup>

In the original x-ray study by Noheda *et al.*<sup>2</sup> the unit cell of the low-temperature monoclinic phase (now usually designated  $M_A$ <sup>5</sup>) was found to be doubled with respect to the primitive cell, with the monoclinic  $a$  and  $b$  axes directed along the  $[110]$  and  $[\bar{1}\bar{1}0]$  axes of the latter ( $a_M \approx b_M \approx a_0\sqrt{2}$ ,  $c_M \approx a_0$ , space group  $Cm$ ). Based upon the atomic positions determined from Rietveld analysis of the synchrotron x-ray data from PbZr

$_{0.52}\text{Ti}_{0.48}\text{O}_3$ , it was concluded<sup>3</sup> that at 20 K the polar axis was tilted about  $24^\circ$  from the [001] axis towards the pseudocubic [111] axis. The structure can be regarded as a condensation of either the local displacements present in the tetragonal  $P4mm$  phase along one of the  $\langle 110 \rangle$  directions, or alternatively those present in the rhombohedral  $R3m$  phase along one of the  $\langle 100 \rangle$  directions, as inferred by Corker *et al.*<sup>8</sup>

However, it is clear that there is a missing ingredient in this simple picture, for in a neutron powder diffraction study of the same sample, Noheda *et al.* reported the presence of one very weak superlattice peak at 20 K corresponding to a doubling of the  $c$  axis of this monoclinic cell, but did not identify the nature of this additional distortion.<sup>6</sup> A similar cell-doubled phase was also observed for  $x = 0.48$  by Ragini and coworkers in electron diffraction patterns below 200 K, but not in their low-temperature x-ray patterns.<sup>18</sup> Based on a subsequent Rietveld analysis of neutron powder data collected at 10 K, the structure of this new phase was reported by Ranjan *et al.* to be monoclinic, with space group  $Pc$ .<sup>19</sup> The appearance of the weak superlattice reflections was attributed to antiphase tilting of the oxygen octahedra about the [001] direction, corresponding to an R-point instability in the cubic Brillouin zone. It was later reported that the correct space group for this proposed model was in fact  $Cc$ ,<sup>20</sup> and a modified set of refined structural parameters was presented.

The  $x = 0.48$  composition has also been the subject of a recent low-temperature neutron powder study by Frantti and colleagues.<sup>21</sup> They, too, note the presence of similar superlattice reflections, but reach very different conclusions; namely that these reflections are attributable to a minority rhombohedral phase with  $R3c$  symmetry in coexistence with the monoclinic  $Cm$  phase, a model that was not considered by Ranjan *et al.*<sup>19</sup> or Hatch *et al.*<sup>20</sup> In a footnote to their paper, Frantti *et al.* comment that the monoclinic  $Pc$  and  $Cc$  models proposed by the latter authors predict peaks that are not observed experimentally, and that the observed superlattice peaks can be accounted for by the  $R3c$  phase. However, this conclusion was not supported by the results obtained by Noheda *et al.*<sup>22</sup> in an electron diffraction study of the same  $x = 0.48$  sample used in the earlier x-ray study,<sup>3</sup> which showed no evidence for a rhombohedral phase, but instead the monoclinic  $Cm$  phase in coexistence with nanoregions of a minority  $Cc$  phase ranging in size from 30-100 Å. These conclusions have been questioned by Frantti *et al.*, who comment that their neutron data provide no evidence of a  $Cc$  phase, and argue that since electron diffraction probes only small volumes of the sample, it is generally not suitable for the determination of average symmetry, and furthermore that the ion-milling technique used for sample thinning is a very violent one which can easily generate significant defects.

In the light of these different interpretations, we have undertaken a detailed Rietveld analysis of the neutron data cited by Noheda *et al.*<sup>6</sup> in an attempt to discrim-

inate between the three models described above. Plausible results were obtained in all three cases, illustrating how difficult it is to identify the correct structural model in complex systems of this type simply on the basis of the standard goodness-of-fit criteria. Nevertheless, we conclude that, taken in conjunction with the electron diffraction data, the results point strongly towards the coexistence model of  $Cm$  and minority  $Cc$  phases.

## II. EXPERIMENTAL

The sample consisted of about 4 g of sintered pellets roughly 1 cm in diameter and 1 mm thick from the same batch of material used in the previous x-ray study.<sup>3</sup> Long-range fluctuations in the composition of the x-ray sample,  $\Delta x$ , were estimated to be less than  $\pm 0.003$  based upon an analysis of the peak widths. The pellets were loaded into a thin-walled vanadium can and mounted in a closed-cycle helium cryostat. Data were collected at the NIST reactor on the powder diffractometer BT1 with a Cu monochromator set for a wavelength of 1.54 Å, collimation of  $15'$  and  $40'$  before and after the monochromator, and  $10'$  in front of each of the 32  $^3\text{He}$  detectors. With this configuration, the best angular resolution attained is about  $0.2^\circ$  at  $2\theta \approx 80^\circ$  ( $\Delta d/d \approx 2 \times 10^{-3}$ ).

Extended data sets were collected at  $2\theta$  step intervals of  $0.05^\circ$  in the monoclinic region at 20 K, in the vicinity of the monoclinic-tetragonal transition at 325 K, and in the tetragonal region at 550 K. Analysis of the data was carried out with the FULLPROF program,<sup>23</sup> using the pseudo-Voigt peak-shape function with appropriate corrections for instrumental asymmetric broadening,<sup>24</sup> and linear interpolation between background points. Particular attention was paid to the problem of anisotropic peak-broadening, which reflects the fact that closely-adjacent peaks may have markedly different widths arising from local strains or compositional fluctuations, for example, as previously noted for PZT and related piezoelectric systems.<sup>2,6,16,25</sup> In standard Rietveld analysis the peak widths are assumed to vary smoothly as a function of scattering angle, and it is important to note that anisotropic peak-broadening due to microstructural effects can be mistakenly interpreted as a symmetry-lowering distortion of the unit cell of the average long-range structure. With the rapidly increasing use of high-resolution x-ray and neutron techniques, it is becoming clear that anisotropic peak-broadening is a common feature of powder diffraction patterns, and should be allowed for as appropriate. One convenient way to do this is provided by the phenomenological model recently proposed by Stephens,<sup>26</sup> in which the broadening is represented by a series of coefficients  $\sum_{HKL} S_{HKL} h^H k^K l^L$  ( $H + K + L = 4$ ), which take into account the Laue symmetry of the space group and are incorporated as refinable parameters in the Rietveld program. For tetragonal  $4mm$  and monoclinic  $2/m$  symmetry, there are respectively 4 and 9 such coefficients.

The data analysis is now described in detail for the tetragonal phase at 550 K, the monoclinic phase at 20 K, and the intermediate region at 325 K.

### A. 550 K

All the peaks could be unambiguously indexed in terms of a tetragonal cell with  $a = 4.060$ ,  $c = 4.100$  Å, except for two very weak peaks attributable to the vanadium sample holder, which were excluded from the analysis. Rietveld refinement was carried out with individual isotropic temperature factors assigned and the atoms placed in the following positions of space group  $P4mm$ : Zr/Ti and O(1) in 1(a) sites at  $0, 0, z$ ; O(2) in 2(c) sites at  $0.5, 0, z$ ; and Pb statistically distributed among the 4(d) sites at  $x, x, 0$ . The Pb positions correspond to random displacements in the  $\langle 110 \rangle$  directions away from the origin, as noted in the previous synchrotron x-ray study.<sup>3</sup> The refinement converged rapidly and smoothly to a goodness-of-fit  $\chi^2$  value of 1.30. However, as in the x-ray study, an examination of the observed and calculated peak profiles revealed a number of systematic discrepancies indicative of anisotropic peak broadening, and additional refinements were carried out in which various combinations of the four possible coefficients were allowed to vary. A definite improvement was obtained when  $S_{004}$  was varied alone ( $\chi^2 = 1.20$ ), but the results obtained with additional coefficients were judged to be of dubious significance, and these coefficients were accordingly set to zero. This result most likely reflects the sensitivity of the  $c$  lattice parameter to the presence of long-range compositional fluctuations. The final refinement results based on this model are listed in Table I, and the profile and difference plots are shown in Fig. 2.

### B. 20 K

A series of refinements was carried out for each of the three models described in the Introduction, namely: single-phase  $Cc$ , two-phase  $Cm/Cc$ , and two-phase  $Cm/R3c$ . However, instead of  $Cc$ , the non-conventional space group setting  $Ic$  was chosen, which has the distinct advantage of having a near-orthogonal unit cell closely related to the  $Cm$  cell, in which the mirror plane is replaced by a  $c$ -glide plane and the  $c$  axis is doubled. The unit-cell axes are related via the transformation  $\mathbf{a}_I = -\mathbf{c}_C$ ,  $\mathbf{b}_I = \mathbf{b}_C$ ,  $\mathbf{c}_I = \mathbf{a}_C + \mathbf{c}_C$ , where the subscripts refer to the unit cells of the  $Ic$  and  $Cc$  space groups respectively. In this setting, it is much easier to visualize the small displacements from the ideal  $Cm$  atomic positions. In the  $Ic$  cell, the Pb atom was chosen to lie at the origin, with Zr/Ti and three inequivalent O atoms in fourfold general positions at  $x, y, z$  and  $x, -y, 1/2 + z$ , and at the related body-center sites. The Zr/Ti and O(1) atoms are in positions similar to those in the  $Cm$  structure at  $x, 0, z$ , the main difference being that they are no longer required

to lie on a mirror plane at  $y = 0$ . The O(2) and O(3) atoms are in two sets of positions derived from the  $x, y, z$  sites and the symmetry-equivalent mirror plane sites at  $x, -y, z$  in the  $Cm$  structure.

#### 1. Single-phase $Ic$ model

In the first series of refinements the atoms were initially assigned the positions found in our previous x-ray study<sup>3</sup> with the exception of the O(2) and O(3) atoms, which were displaced from the ideal  $Cm$  positions by small shifts corresponding to antiphase tilting of the oxygen octahedra about the [001] axis, as assumed by Ranjan *et al.*<sup>19</sup> The corresponding positions chosen for O(2) and O(3) in the  $Ic$  structure were  $x - \delta, y - \delta, z/2$  and  $1/2 + x + \delta, 1/2 + y + \delta, z/2$ , where  $\delta$  is the shift in the  $x$  and  $y$  directions due to tilting. It is important to note that with such a constrained-tilt, rigid-octahedron model, the  $x$  and  $y$  values assumed for the O(2) and O(3) positions (in this case the  $Cm$  values found in the previous x-ray study) do not change in the course of the refinement. The resulting fit was reasonably good ( $\chi^2 = 1.97$ ), but inspection of the individual peak profiles once again revealed some significant discrepancies due to anisotropic peak broadening. As before, a distinct improvement was obtained when the anisotropy coefficient  $S_{004}$  was refined ( $\chi^2 = 1.78$ ), but further refinements with various combinations of the other eight anisotropy coefficients gave only minimally improved fits, and the one-parameter anisotropy model was accordingly adopted for subsequent refinements. At this point, the constraints on the Zr/Ti and O(1)  $y$  parameters were relaxed, but the shifts from the ideal positions at  $y = 0$  and the improvement in the overall fit were judged to be insignificant. A similar result was obtained when the Zr/Ti compositional parameter  $x$  was varied.

Further refinements were performed, first with constrained models corresponding to rigid-octahedron tilting about the [111] and [110] axes respectively, and finally, with all the constraints on the O(2) and O(3) positions removed. In the latter case, the refinement proceeded smoothly and converged rapidly to a set of positions which were much closer to those of the [001]-tilt model than the other tilt models independent of which tilt model was used to provide the initial values of the positions. However, in none of these cases did the overall fit appear to be significantly improved, and we therefore conclude that the [001]-tilt model is a reasonable choice, although it is clearly not possible to rule out the other models on the basis of the present data. The final refinement was therefore carried out for the constrained [001]-tilt model, but with the  $x$  and  $y$  values for O(2) and O(3) derived from the results for the unconstrained model. This refinement yielded a  $\chi^2$  value of 1.52, with refined parameters as listed in Table II (column 1). Also shown are the values reported by Hatch *et al.*<sup>20</sup> transformed from  $Cc$  to  $Ic$  symmetry (column 3). From a

comparison of the two sets of atomic positions, it appears that the constraints applied by Hatch *et al.* do not in fact correspond to an [001]-tilt model, but instead to a simpler model in which only the  $y$  parameters of the O(2) and O(3) atoms are displaced from their ideal  $Cm$  positions. An additional refinement based on such a  $y$ -shift model yielded results which are seen to be in excellent agreement with those of Hatch *et al.* (column 2 of Table II), although the fit is somewhat inferior to that given by the [001]-tilt model ( $\chi^2 = 1.62$ ). It is also worth noting that the values of axial ratio,  $c_0/a_0$ , and the pseudocubic cell volume,  $V_0$ , obtained by the latter authors suggest a slightly higher Zr content ( $\approx 0.5\%$ ) relative to the present sample.<sup>6,21</sup>

From the atomic positions listed in the first column of Table II the octahedral tilt angle is calculated as about  $3^\circ$ . The polar displacements of the Zr/Ti and Pb atoms with respect to the respective polyhedra centers are  $-0.08$  and  $-0.22$  Å along monoclinic [100], and  $0.18$  and  $0.44$  Å along [001], corresponding to a rotation of the polar axis towards pseudocubic [111] of roughly  $25^\circ$ . However, these values are representative only of the average long-range structure, since they do not allow for the local distortions revealed in the PDF analysis cited earlier.<sup>14</sup>

## 2. Two-phase $Cm/R3c$ model

The next set of refinements was performed for the two-phase  $Cm/R3c$  model favored by Frantti *et al.*<sup>21</sup> Significantly better peak profiles were obtained with an anisotropic-broadening model for the  $Cm$  phase in which  $S_{004}$  was allowed to vary, together with an isotropic particle-size broadening coefficient for the  $R3c$  phase. The refinement converged rapidly to a  $\chi^2$  value of 1.27 with the final parameters as listed in Table III. The latter are in close agreement with those reported by Frantti *et al.*, including the respective weight fractions of the two phases. Compared to the single-phase  $Ic$  model, the overall fit is considerably better ( $\chi^2 = 1.27$  vs. 1.52), but because several additional variable parameters are involved, it is difficult to judge the true significance of this result. Inspection of the results listed in Table III reveals that in both samples,  $V_0$  for the rhombohedral phase is larger by about  $0.3$  Å<sup>3</sup>, which would imply a significantly higher Zr content of some 3-4%.<sup>6,21</sup> For the present sample, at least, such a conclusion would be inconsistent with the previously estimated long-range compositional fluctuations.<sup>3</sup>

## 3. Two-phase $Cm/Ic$ model

The final set of refinements was carried out for the two-phase  $Cm/Ic$  model deduced by Noheda *et al.* from the results of an electron diffraction study.<sup>22</sup> Since we did not anticipate that a meaningful result would be obtained for an unconstrained refinement of two such

closely-related structures, a highly constrained model was used; namely, the atomic positions in the  $Cm$  and  $Ic$  phases were constrained to be equivalent except for one additional parameter  $\delta$  for the latter representing the displacement along the  $x$  and  $y$  axes for the idealized [001]-tilt model described above. The peak-shape model, including an  $S_{004}$  anisotropy coefficient, was also constrained to be equivalent for both phases, except for an isotropic particle-size broadening coefficient which was included for the  $Ic$  phase. The refined values for the two phases are listed side-by-side in Table IV for easy comparison, and the profile fit and difference plot are shown in Fig. 3. The relative proportions of the  $Cm$  and  $Ic$  phases are approximately 4:1 and thus consistent with the electron diffraction results, but the estimated particle size derived from the broadening coefficient is much larger, about 1000 Å compared to 100 Å. As pointed out by Frantti *et al.*,<sup>21</sup> this discrepancy could arise because of the ion-milling techniques used to thin the electron diffraction sample, which can generate significant numbers of defects.

Detailed comparison of the results in Tables II, III and IV reveals that a better fit is obtained with the two-phase  $Cm/Ic$  model ( $\chi^2 = 1.16$ ,  $R_{wp} = 0.064$ ) than with the  $Cm/R3c$  model ( $\chi^2 = 1.27$ ,  $R_{wp} = 0.067$ ) or the single-phase  $Ic$  model ( $\chi^2 = 1.52$ ,  $R_{wp} = 0.073$ ), but it would nevertheless be premature to conclude that the former must therefore be correct, since there are no generally-accepted statistical tests to judge the true significance of the results. However, although the extended profile and difference plots for the two latter models are hardly distinguishable by eye from those shown in Fig. 3, there are significant differences in some of the individual peak profiles which provide additional insight, as shown in Figs. 4 and 5 respectively. Fig. 4 shows the region around the strongest superlattice peak at  $2\theta \approx 36.8^\circ$ , from which it is evident that a much better fit is obtained with the  $Ic$  and  $Cm/Ic$  models than with the  $Cm/R3c$  model. On the other hand, the fit shown in Fig. 5 in the pseudocubic (200) region reveals serious deficiencies for the  $Ic$  model compared to the  $Cm/R3c$  and particularly the  $Cm/Ic$  model, which accounts much better for the asymmetry of the profiles in the central region.

We note also that further analysis of the synchrotron x-ray data reported in Ref. 3 shows that the  $Cm/Ic$  co-existence model is superior to the two-phase  $Cm/Pm3m$  model previously used, with  $\chi^2$  values of 7.3 and 12.8 respectively. The results are in reasonable agreement with those of the neutron study; in particular, the ratio of the two phases is found to be about 4:1, very similar to the value listed in Table IV. The failure to detect any superlattice peaks analogous to the one in the neutron pattern can be explained by the relatively much weaker x-ray scattering power of oxygen compared to Pb and Zr/Ti, resulting in calculated intensities that are insignificant compared to the background signal.

From the atomic positions listed in Table IV, the octahedral tilt angle about the [001] axis is calculated as

about  $7^\circ$ . The polar shifts of the Zr/Ti and Pb atoms with respect to the polyhedra centers are essentially the same as those obtained for the single-phase  $Ic$  refinement. It is also seen that the values of the cell volume  $V_0$  and the axial ratio  $c_0/a_0$  for the  $Ic$  phase are respectively slightly larger and smaller than those for  $Cm$ , and thus suggestive of a slightly higher Zr content ( $\approx 0.5\%$ ) for the former.<sup>6,21</sup>

### C. 325 K

Refinement was first carried out based on a model similar to that used for the 550 K data; namely, a single-phase tetragonal structure with  $P4mm$  symmetry, Pb atoms statistically distributed among the 4(d) sites at  $x, x, 0$ , and a single anisotropy-broadening coefficient,  $S_{004}$ . However, the overall fit was only mediocre ( $\chi^2 = 2.94$ ,  $R_{wp} = 0.072$ ), and a detailed inspection of the individual peak profiles revealed asymmetries consistent with the presence of a monoclinic component. Such a coexistence model of monoclinic and tetragonal phases for  $x = 0.48$  at room temperature was proposed in an earlier neutron study by Frantti *et al.*,<sup>27</sup> and in a more recent x-ray study by Ragini *et al.*<sup>28</sup> Further refinements based on this model gave a markedly improved fit ( $\chi^2 = 1.76$ ,  $R_{wp} = 0.056$ ), but some residual diffuse scattering was clearly present between some of the peaks. This scattering is probably associated with locally disordered regions in the vicinity of domain walls and can be modeled in a simple, albeit rather artificial, way by the addition of a cubic phase with  $Pm3m$  symmetry, as assumed in our previous x-ray study.<sup>3</sup> Such a three-phase model yielded a reasonably satisfactory fit ( $\chi^2 = 1.47$ ,  $R_{wp} = 0.051$ ), with weight fractions of tetragonal, monoclinic and cubic phases in the ratio 0.61:0.33:0.06.

The refined parameters are listed in Table V, and the profile fit and difference plot are shown in Fig. 6. Also listed are the parameters reported by Ragini *et al.*<sup>18</sup> and Frantti *et al.*<sup>21</sup> In the latter case, it is rather surprising in the light of the results reported in Ref. 6 that the lattice strain  $c_0/a_0$  was found to be significantly larger for the monoclinic phase than for the tetragonal one, since one would not expect rotation of the polarization direction away from [001] in the monoclinic phase to increase this strain. Other than this, the three sets of parameters are in reasonable agreement except that the fraction of  $Cm$  phase in the room temperature studies is considerably larger than at 325 K, as would be expected.

Further analysis of the earlier x-ray data<sup>3</sup> revealed that this three-phase model gives a noticeably better profile fit than that obtained with the two-phase  $P4mm/Pm3m$  model previously used, with  $\chi^2$  values of 7.5 and 9.9 respectively. The weight fractions of the three phases were in the ratio 0.55:0.40:0.05, comparable to the neutron values listed in Table V. We emphasize, however, that these results should be regarded as representative only of an average long-range structure, since the true

nature of the material in the transition region is surely far more complex than implied by a simple three-phase model. It is more likely in this temperature interval that small fluctuations in composition lead to coexistence of the tetragonal phase with locally-ordered monoclinic regions of widely varying sizes and possibly some disordered regions.

### III. DISCUSSION

In summary, the results obtained in the present neutron investigation are consistent with the coexistence of majority  $Cm$  and minority  $Ic$  phases in  $\text{PbZr}_{0.52}\text{Ti}_{0.48}\text{O}_3$ , in agreement with the results of a recent electron diffraction study of the same sample. The  $Cm$  ( $M_A$ ) phase, which plays a key role in the piezoelectric and ferroelectric behavior of PZT and related systems is the majority phase at low temperature. The structure of the minority  $Ic$  phase is readily visualized as the superposition of an antiphase octahedral-tilt system on the parent  $Cm$  structure. Furthermore, the close agreement between the refinement results for the alternative  $Ic$  and  $Cm/R3c$  models and those in Refs. 20 and 21 respectively suggests that the two-phase  $Cm/Ic$  model is worth consideration in those cases as well. It is possible that the coexistence of  $Cm$  and  $Ic$  phases in the present  $x = 0.48$  sample reflects the existence of a narrow thermodynamically-stable region with  $Ic$  symmetry at low temperature somewhere between  $0.45 < x < 0.48$ . In this case, the coexistence of  $Ic$  and  $Cm$  phases could plausibly be attributed to the presence of long-range compositional fluctuations, as suggested by the values of the lattice parameters for the two-phase refinement in Table V. In this context, it is interesting to note that recent neutron data obtained by Frantti *et al.* for a sample with  $x = 0.46$  show clear evidence of a superlattice peak at 4 K.<sup>29</sup> However, the authors interpret this as evidence for the coexistence of  $Cm$  and  $R3c$  phases, and did not consider the possibility of  $Cm$  and  $Ic$  phase coexistence. Alternatively, the  $Ic$  phase could be a metastable one resulting from the presence of local strains at domain-wall boundaries, for example. Indeed, it is noteworthy that first-principles calculations by Fornari and Singh have shown that local stress fields may lead to the coexistence of both ferroelectric and rotational instabilities near the MPB.<sup>30</sup> In any case, it is clear that a very careful high-resolution x-ray, neutron and electron diffraction study of extremely well-characterized samples would be required in order to throw further light on these issues.

On a final note of caution, the present study also demonstrates that the interpretation of the results of Rietveld analysis may be very tricky for complex systems such as this one in which allowance must be made for the possible coexistence of closely-related phases and the presence of anisotropic peak broadening. The choice of any particular model should take into account not only the quality of the refinement as judged by the agreement

factors and goodness-of-fit, but also the diffraction profiles of alternative models in selected key regions of the pattern, and, if feasible, data from complimentary structural techniques such as electron diffraction.

### ACKNOWLEDGMENTS

We would like to acknowledge the support of the NIST

Center for Neutron Research, U. S. Department of Commerce, and to thank B. H. Toby for experimental assistance at beamline BT1. Financial support from the U.S. Department of Energy, Division of Materials Sciences, under contract No. DE-AC02-98CH10886 is also acknowledged.

- 
- \* Present address: Materials Science Center, University of Groningen, Nijenborgh 4, 9747 AG Groningen, The Netherlands
- <sup>1</sup> B. Jaffe, W. R. Cook, and H. Jaffe, *Piezoelectric Ceramics* (Academic, London, 1971).
  - <sup>2</sup> B. Noheda, D.E. Cox, G. Shirane, J.A. Gonzalo, L.E. Cross, and S-E. Park, *Appl. Phys. Lett.* **74**, 2059 (1999).
  - <sup>3</sup> B. Noheda, J.A. Gonzalo, L.E. Cross, R. Guo, S-E. Park, D.E. Cox, and G. Shirane, *Phys. Rev. B* **61**, 8687 (2000).
  - <sup>4</sup> L. Bellaiche, A. Garcia, and D. Vanderbilt. *Phys. Rev. Lett.* **84**, 5427 (2000).
  - <sup>5</sup> D. Vanderbilt and M.H. Cohen, *Phys. Rev. B* **63**, 094108 (2001).
  - <sup>6</sup> B. Noheda, D.E. Cox, G. Shirane, R. Guo, B. Jones, and L.E. Cross, *Phys. Rev. B* **63**, 014103 (2001).
  - <sup>7</sup> C. Michel, J. M. Moreau, G. D. Achenbach, R. Gerson, and W. J. James, *Solid State Commun.* **7**, 865 (1969).
  - <sup>8</sup> D. L. Corker, A.M. Glazer, R.W. Whatmore, A. Stalard, and F. Fauth, *J. Phys.: Condensed Matter* **10**, 6251 (1998).
  - <sup>9</sup> D. Viehland, *Phys. Rev. B* **52**, 778 (1995).
  - <sup>10</sup> D. Viehland, J-F. Li, X. Dai, and Z. Xu, *J. Phys. Chem. Solids* **57**, 1545 (1996).
  - <sup>11</sup> J. Ricote, D. L. Corker, R.W. Whatmore, S. A. Impey, A.M. Glazer, J. Dec, and K. Roleder, *J. Phys.: Condensed Matter* **10**, 1767 (1998).
  - <sup>12</sup> S. Teslic, T. Egami, and D. Viehland, *J. Phys. Chem. Solids* **57**, 1537 (1996).
  - <sup>13</sup> S. Teslic, T. Egami, and D. Viehland, *Ferroelectrics* **194**, 271 (1997).
  - <sup>14</sup> W. Dmowski, T. Egami, L. Farber, and P. K. Davies, in *Fundamental Physics of Ferroelectrics - Eleventh Williamsburg Ferroelectrics Workshop*, edited by H. Krakauer, AIP Conf. Proc. No. 582 (AIP, Woodbury, NY, 2001), p. 33.
  - <sup>15</sup> J. Frantti, J. Lappalainen, V. Lantto, S. Nishio, and M. Kakihana, *Jpn. J. Appl. Phys.* **38**, 5679 (1999).
  - <sup>16</sup> J. Frantti, S. Ivanov, J. Lappalainen, S. Eriksson, V. Lantto, S. Nishio, M. Kakihana, and H. Rundlöf, *Ferroelectrics* **266**, 73 (2002).
  - <sup>17</sup> I. Grinberg, V. R. Cooper, and A. M. Rappe, *Nature* **419**, 909 (2002).
  - <sup>18</sup> Ragini, S. K. Mishra, D. Pandey, H. Lemmens, and G. Van Tendeloo, *Phys. Rev. B* **64**, 054101 (2001).
  - <sup>19</sup> R. Ranjan, Ragini, S. K. Mishra, D. Pandey, and B. J. Kennedy, *Phys. Rev. B* **65**, 060102 (2002).
  - <sup>20</sup> D. M. Hatch, H. T. Stokes, R. Ranjan, Ragini, S. K. Mishra, D. Pandey, and B. J. Kennedy, *Phys. Rev. B* **65**, 212101 (2002).
  - <sup>21</sup> J. Frantti, S. Ivanov, S. Eriksson, H. Rundlöf, V. Lantto, J. Lappalainen, and M. Kakihana, *Phys. Rev. B* **66**, 064108 (2002).
  - <sup>22</sup> B. Noheda, L. Wu, and Y. Zhu, *Phys. Rev. B* **66**, 060103 (2002).
  - <sup>23</sup> J. Rodriguez-Carvajal, Program FULLPROF, version 1.9c (2001). Available by anonymous ftp from [www.charybde.saclay.cea.fr/pub/divers/](http://www.charybde.saclay.cea.fr/pub/divers/).
  - <sup>24</sup> L. W. Finger, D. E. Cox, and A. W. Jephcoat, *J. Appl. Cryst.* **27**, 892 (1994).
  - <sup>25</sup> J-M. Kiat, Y. Uesu, B. Dkhil, M. Matsuda, C. Malibert, and G. Calvarin, *Phys. Rev. B* **65**, 064106 (2002).
  - <sup>26</sup> P. W. Stephens, *J. Appl. Cryst.* **32**, 281 (1999).
  - <sup>27</sup> J. Frantti, J. Lappalainen, S. Eriksson, V. Lantto, S. Nishio, M. Kakihana, S. Ivanov, and H. Rundlöf, *Jpn. J. Appl. Phys.* **39**, 5697 (2000).
  - <sup>28</sup> Ragini, R. Ranjan, S. K. Mishra, and D. Pandey, *J. Appl. Phys.* **92**, 3266 (2002).
  - <sup>29</sup> J. Frantti, S. Eriksson, S. Hull, V. Lantto, H. Rundlöf, and M. Kakihana, *J. Phys.: Condensed Matter* **15**, 6031 (2003).
  - <sup>30</sup> M. Fornari and D. J. Singh, *Phys. Rev. B* **63**, 092101 (2001).

TABLE I: Refined structural parameters for tetragonal  $\text{PbZr}_{0.52}\text{Ti}_{0.48}\text{O}_3$  at 550 K, space group  $P4mm$ , lattice parameters  $a = 4.0596(1)$ ,  $c = 4.0999(1)$  Å. The refinement was based on a model with the Pb atoms statistically distributed among 4(d) sites at  $x, x, 0$ , corresponding to local displacements along (110) directions. Figures in parentheses denote standard errors referred to the least significant digit.  $R_{wp}$ ,  $R_B$  and  $\chi^2$  are agreement factors as defined in Ref. 23.

	$x$	$y$	$z$	$U(\text{Å}^2)$
Pb	0.033(1)	0.033(1)	0.0	0.028(1)
Zr/Ti	0.5	0.5	0.450(2)	0.005(1)
O(1)	0.5	0.5	-0.061(1)	0.027(1)
O(2)	0.5	0.0	0.427(1)	0.027(1)
$R_{wp}$		0.048		
$R_B$		0.034		
$\chi^2$		1.20		

TABLE II: Refined structural parameters for monoclinic  $\text{PbZr}_{0.52}\text{Ti}_{0.48}\text{O}_3$  at 20 K, single-phase model with space group  $Ic$ , for the [001]-tilt and  $y$ -shift models described in the text. The Pb atom was fixed at the origin, and the O(2) and O(3) temperature factors were constrained to be equal. Also listed are the parameters recently reported by Hatch *et al.*<sup>20</sup>, but with the values transformed from  $Cc$  to  $Ic$  symmetry.  $V_0$  and  $c_0/a_0$  represent respectively the volume and axial ratio of the primitive pseudocubic cell, with  $c_0 = c/2$  and  $a_0 = (a + b)/2\sqrt{2}$ .

	Present study		Hatch <i>et al.</i>
	[001]-tilt	$y$ -shift	$y$ -shift
$a(\text{Å})$	5.7131(1)	5.7131(1)	5.7312(7)
$b(\text{Å})$	5.7000(1)	5.7001(1)	5.7093(6)
$c(\text{Å})$	8.2679(2)	8.2683(3)	8.2363(7)
$\beta(^{\circ})$	90.475(2)	90.473(2)	90.50(1)
$V_0(\text{Å}^3)$	67.31	67.31	67.37
$c_0/a_0$	1.0245	1.0246	1.0181
Pb: $U(\text{Å}^2)$	0.013(1)	0.012(1)	0.013(1)
Zr/Ti: $x$	0.524(2)	0.524(2)	0.519(5)
$z$	0.219(1)	0.218(1)	0.216(2)
$U(\text{Å}^2)$	0.002(1)	0.003(2)	0.006(4)
O(1): $x$	0.542(1)	0.543(1)	0.548(3)
$z$	-0.046(1)	-0.046(1)	-0.044(1)
$U(\text{Å}^2)$	0.011(1)	0.011(1)	0.011(3)
O(2): $x$	0.275(1)	0.287(1)	0.289(2)
$y$	0.243(1)	0.233(1)	0.233(1)
$z$	0.193(1)	0.194(1)	0.196(1)
$U(\text{Å}^2)$	0.010(1)	0.011(1)	0.009(1)
O(3): $x$	0.801(1)	0.787(1)	0.789(2)
$y$	0.768(1)	0.767(1)	0.767(1)
$z$	0.193(1)	0.194(1)	0.196(1)
$U(\text{Å}^2)$	0.010(1)	0.011(1)	0.009(1)
$R_{wp}$	0.073	0.076	0.086
$R_B$	0.041	0.047	0.040
$\chi^2$	1.52	1.62	1.21

TABLE III: Refined structural parameters for  $\text{PbZr}_{0.52}\text{Ti}_{0.48}\text{O}_3$  at 20 K, two-phase model with space groups  $Cm$  and  $R3c$ . The Pb and Zr/Ti atoms were fixed at the origin for the  $Cm$  and  $R3c$  refinements respectively, and the temperature factors for the separate atoms were constrained to be the same in both structures. Also listed are the 10 K parameters recently reported by Frantti *et al.*<sup>21</sup>

	Present study		Frantii <i>et al.</i>	
	$Cm$	$R3c$	$Cm$	$R3c$
$a$ (Å)	5.7120(1)	5.7415(6)	5.7097(7)	5.744(2)
$b$ (Å)	5.6988(1)	-	5.6984(7)	-
$c$ (Å)	4.1353(1)	14.208(3)	4.1367(3)	14.212(8)
$\beta$ (°)	90.479(2)	-	90.449(8)	-
$V_o$ (Å <sup>3</sup> )	67.32	67.60	67.29	67.68
$c_o/a_o$	1.0257	1.0	1.0256	1.0
Pb:				
$z$	-	0.283(4)	-	0.282(5)
$U$ (Å <sup>2</sup> )	0.012(1)	0.012(1)	0.009(1)	0.004(6)
Zr/Ti:				
$x$	0.531(2)	-	0.539(3)	-
$z$	0.441(2)	-	0.441(3)	-
$U$ (Å <sup>2</sup> )	0.004(1)	0.004(1)	0.001(2)	0.001(2)
O(1):				
$x$	0.543(1)	-	0.540(1)	-
$z$	-0.090(1)	-	-0.092(2)	-
$U$ (Å <sup>2</sup> )	0.008(1)	-	0.011(2)	-
O(2):				
$x$	0.288(1)	0.137(3)	0.283(1)	0.148(3)
$y$	0.254(1)	0.347(3)	0.253(1)	0.354(3)
$z$	0.389(10)	0.081(4)	0.388(1)	0.081(6)
$U$ (Å <sup>2</sup> )	0.015(1)	0.015(1)	0.013(1)	0.007(5)
$f$ (wt fraction)	0.89(1)	0.11(1)	0.87	0.13
$R_{wp}$	0.067		0.058	
$R_B$	0.039	0.067	0.042	
$\chi^2$	1.27		2.28	

TABLE IV: Refined structural parameters for monoclinic  $\text{PbZr}_{0.52}\text{Ti}_{0.48}\text{O}_3$  at 20 K, two-phase model with space groups  $Cm$  and  $Ic$ . The atomic positions for  $Ic$  symmetry were based upon the [001]-tilt model described in text and constrained to be equivalent to those for  $Cm$  except for one additional parameter  $\delta$  corresponding to O(2) and O(3) displacements in the  $x$  and  $y$  directions due to tilting. For comparison with the  $Ic$  structure, the O(2) and O(3) positions for the  $Cm$  structure are shown separately, although in fact they are symmetry-equivalent. The temperature factors for the separate atoms were constrained to be the same in both structures.

	$Cm$	$Ic$
$a(\text{\AA})$	5.7097(1)	5.7401(7)
$b(\text{\AA})$	5.6988(1)	5.7188(8)
$c(\text{\AA})$	4.1373(1)	8.2098(11)
$\beta(^{\circ})$	90.473(2)	90.550(10)
$V_o(\text{\AA}^3)$	67.31	67.37
$c_o/a_o$	1.0257	1.0127
Pb: $U(\text{\AA}^2)$	0.012(1)	0.012(1)
Zr/Ti: $x$	0.530(2)	0.530(2)-
$z$	0.437(1)	0.218(1)
$U(\text{\AA}^2)$	0.003(1)	0.003(1)
O(1): $x$	0.541(1)	0.541(1)
$z$	-0.089(1)	-0.045(1)
O(2): $U(\text{\AA}^2)$	0.011(1)	0.011(1)
$x$	0.286(1)	0.257(1)
$y$	0.254(1)	0.225(1)
$z$	0.390(1)	0.195(1)
O(3): $U(\text{\AA}^2)$	0.015(1)	0.015(1)
$x$	0.786(1)	0.814(1)
$y$	0.754(1)	0.783(1)
$z$	0.390(1)	0.195(1)
$U(\text{\AA}^2)$	0.015(1)	0.015(1)
$f(\text{wt fraction})$	0.78(2)	0.22(2)
$R_{wp}$		0.064
$R_B$	0.039	0.053
$\chi^2$		1.16

TABLE V: Refined structural parameters for the  $Cm$  and  $P4mm$  phases in  $PbZr_{0.52}Ti_{0.48}O_3$  at 325 K with the three-phase model described in text. The temperature factors for the separate atoms were constrained to be the same in both structures. Also listed are the room-temperature parameters recently reported in an x-ray study by Ragini *et al.*<sup>28</sup> and in a neutron study by Frantti *et al.*<sup>27</sup> The weight fraction of the cubic  $Pm3m$  phase was determined as 0.06.

	Present study		Ragini <i>et al.</i>		Frantti <i>et al.</i>	
	$Cm$	$P4mm$	$Cm$	$P4mm$	$Cm$	$P4mm$
$a(\text{\AA})$	5.7268(3)	4.0393(1)	5.7520(1)	4.0429(2)	5.7129(3)	4.0550(4)
$b(\text{\AA})$	5.7187(3)	-	5.7431(2)	-	5.7073(3)	-
$c(\text{\AA})$	4.1230(2)	4.1388(1)	4.0912(4)	4.1318(3)	4.1436(1)	4.1097(6)
$\beta(^{\circ})$	90.393(5)	-	90.48(1)	-	90.199(3)	-
$V_o(\text{\AA}^3)$	67.51	67.53	67.57	67.53	67.55	67.58
$c_o/a_o$	1.0189	1.0246	1.0067	1.0219	1.0262	1.0135
Pb:						
$z$	-	0.035(2) <sup>a</sup>	-	-	-	-
$U(\text{\AA}^2)$	0.017(1)	0.017(1)	0.107 <sup>b</sup>	0.030 <sup>c</sup>	0.021 <sup>d</sup>	0.019(1)
Zr/Ti:						
$x$	0.530(4)	-	0.578(3)	-	0.507(2)/0.494(4) <sup>e</sup>	-
$z$	0.432(5)	0.442(2)	0.473(3)	0.447(2)	0.426(1)/0.404(4) <sup>e</sup>	0.431(4)
$U(\text{\AA}^2)$	0.003(1)	0.0043(1)	0.015(1)	0.005(2)	0.004(1)	0.019(1)
O(1):						
$x$	0.540(2)	-	0.50(1)	-	0.522(1)	-
$z$	-0.080(3)	-0.085(2)	-0.10(1)	-0.109(6)	-0.090(1)	-0.080(2)
$U(\text{\AA}^2)$	0.016(1)	0.016(1)	0.00(1)	0.029(1)	0.013(1)	0.019(1)
O(2) :						
$x$	0.287(2)	-	0.36(1)	-	0.270(1)	-
$y$	0.255(1)	-	0.219(8)	-	0.252(1)	-
$z$	0.400(2)	0.0395(1)	0.404(8)	0.389(3)	0.391(1)	0.400(1)
$U(\text{\AA}^2)$	0.021(2)	0.021(2)	0.04(1)	0.029(1)	0.013(1)	0.019(1)
$f$ (wt fraction)	0.33(1)	0.61(2)	0.58	0.42	0.69	0.31
$R_{wp}$	0.051		0.128		0.021	
$R_B$	0.043	0.030	0.041	0.062	-	
$\chi^2$	1.47		3.39		2.69	

(a) Pb atoms statistically distributed among 4(d) sites at  $x, x, 0$ .

(b) Equivalent isotropic  $U$

( $U_{11} = 0.221, U_{22} = 0.027, U_{33} = 0.074, U_{13} = 0.030 \text{ \AA}^2$ ).

(c) Equivalent isotropic  $U$  ( $U_{11} = U_{22} = 0.031, U_{33} = 0.027 \text{ \AA}^2$ ).

(d) Equivalent isotropic  $U$

( $U_{11} = 0.027, U_{22} = 0.026, U_{33} = 0.011, U_{13} = 0.013 \text{ \AA}^2$ ).

(e) Zr and Ti parameters refined independently.

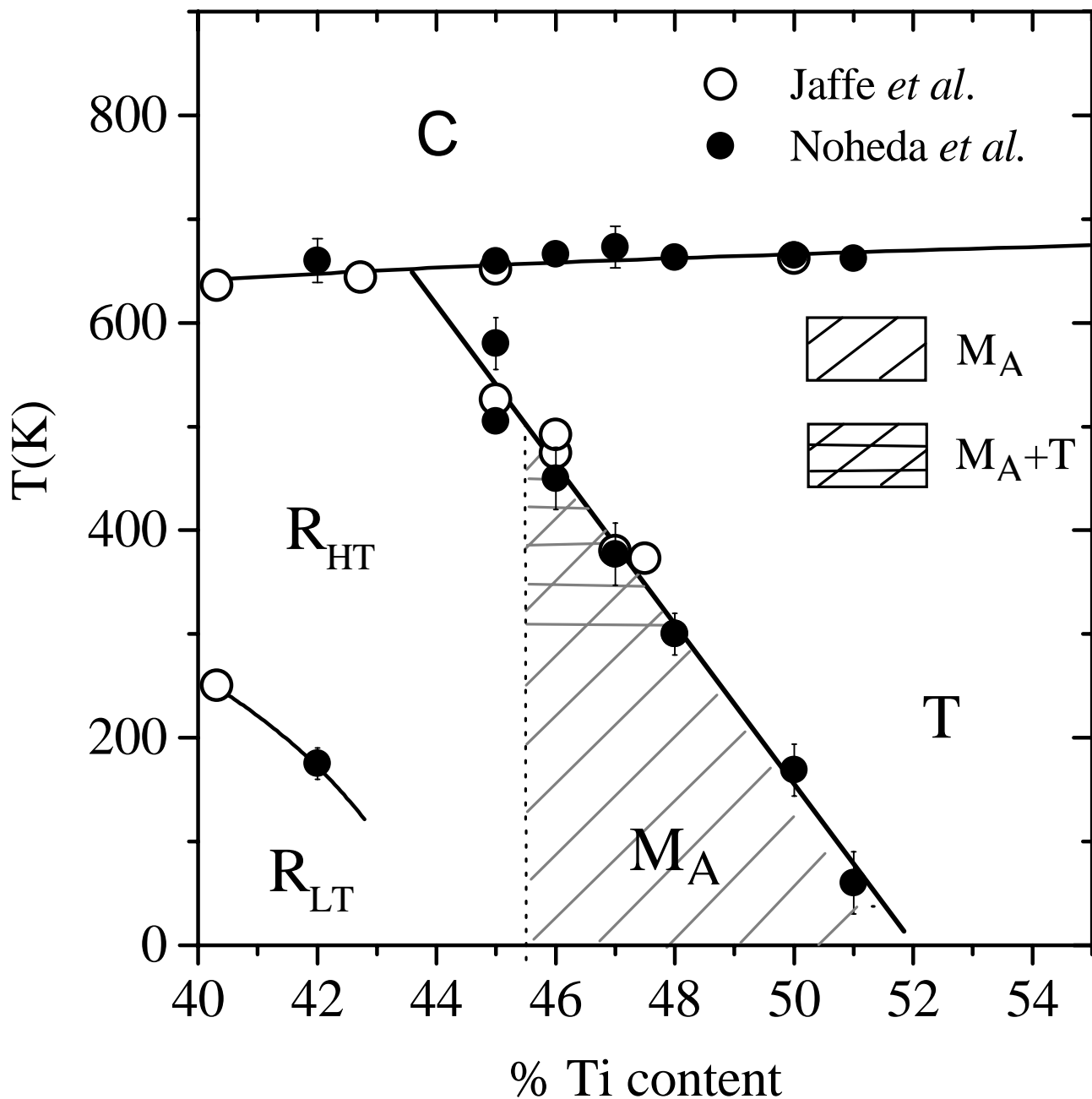
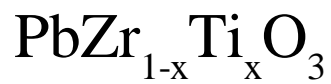


FIG. 1: PZT phase diagram as originally proposed by Jaffe et al. in Ref. 1 (open circles) with the modifications reported by Noheda et al. in Ref. 6 (full circles). The various phases described in the text are denoted by C (cubic  $Pm\bar{3}m$ ),  $R_{HT}$  (rhombohedral  $R\bar{3}m$ ),  $R_{LT}$  (rhombohedral  $R\bar{3}c$ ), T (tetragonal  $P4mm$ ), and  $M_A$  (monoclinic  $Cm$ ).

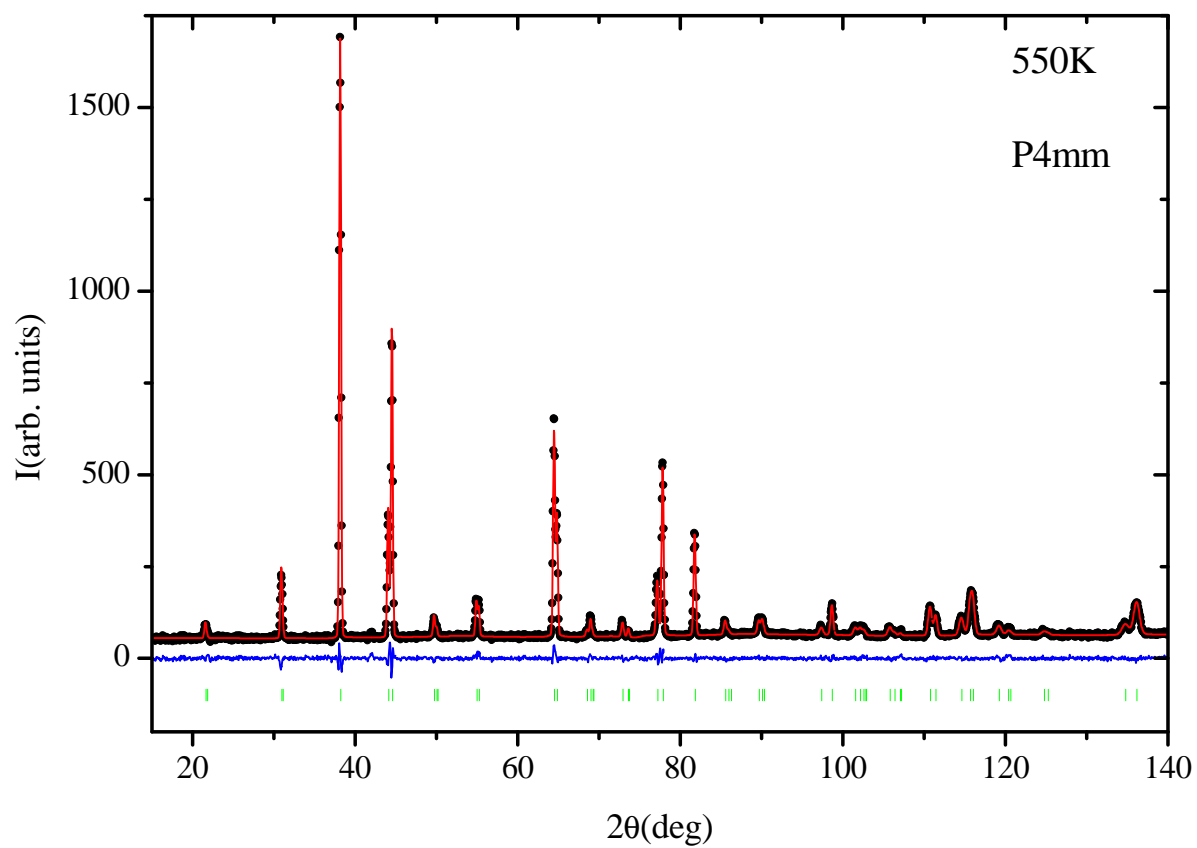


FIG. 2: (Color) Observed and calculated diffraction profiles from the Rietveld refinement of  $\text{PbZr}_{0.52}\text{Ti}_{0.48}\text{O}_3$  at 550 K, with space group  $P4mm$ . The difference plot is shown below, with short vertical markers denoting the calculated peak positions.

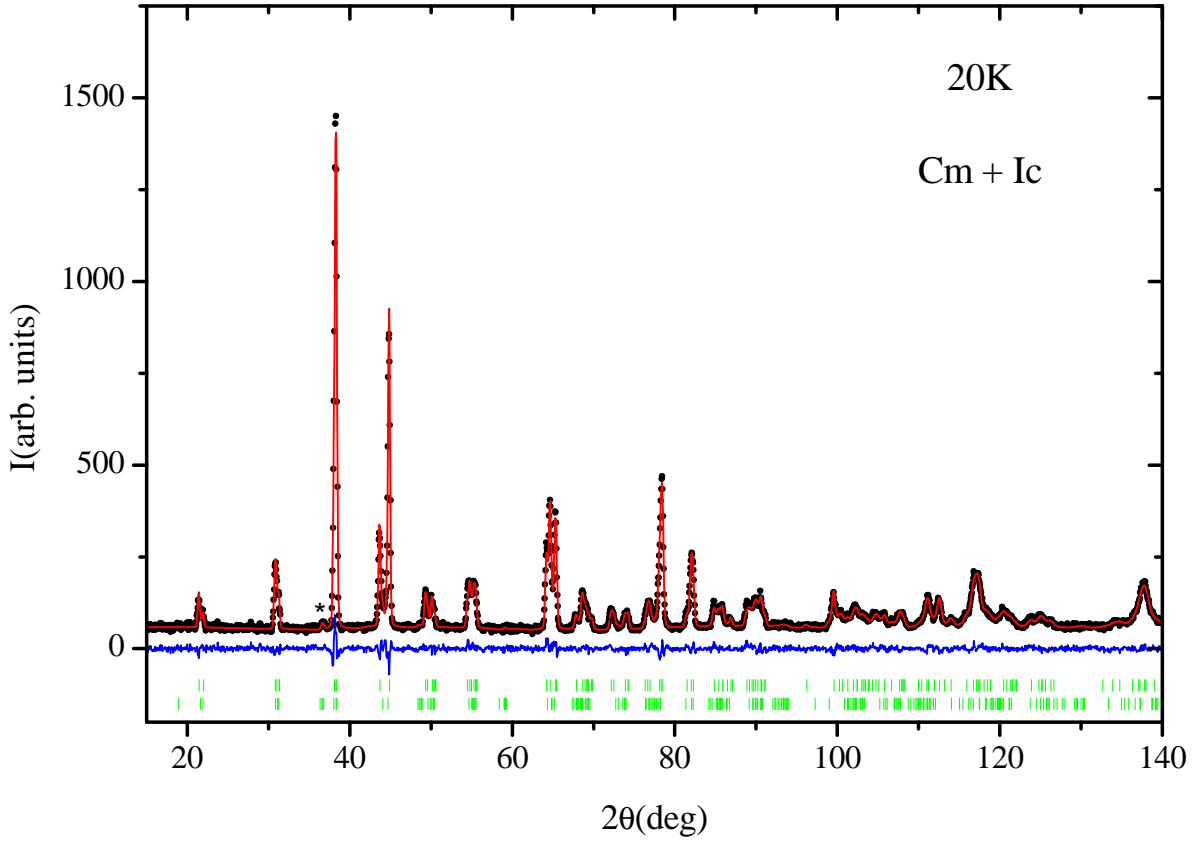


FIG. 3: (Color) Observed and calculated diffraction profiles from the two-phase Rietveld refinement of  $\text{PbZr}_{0.52}\text{Ti}_{0.48}\text{O}_3$  at 20 K, with space groups  $Cm$  and  $Ic$ . The difference plot is shown below, with upper and lower sets of vertical markers denoting the calculated peak positions for  $Cm$  and  $Ic$  respectively. The position of the weak superlattice peak at  $2\theta \approx 36.8^\circ$  (pseudocubic  $3/2 \ 1/2 \ 1/2$ ) is indicated with an asterisk.

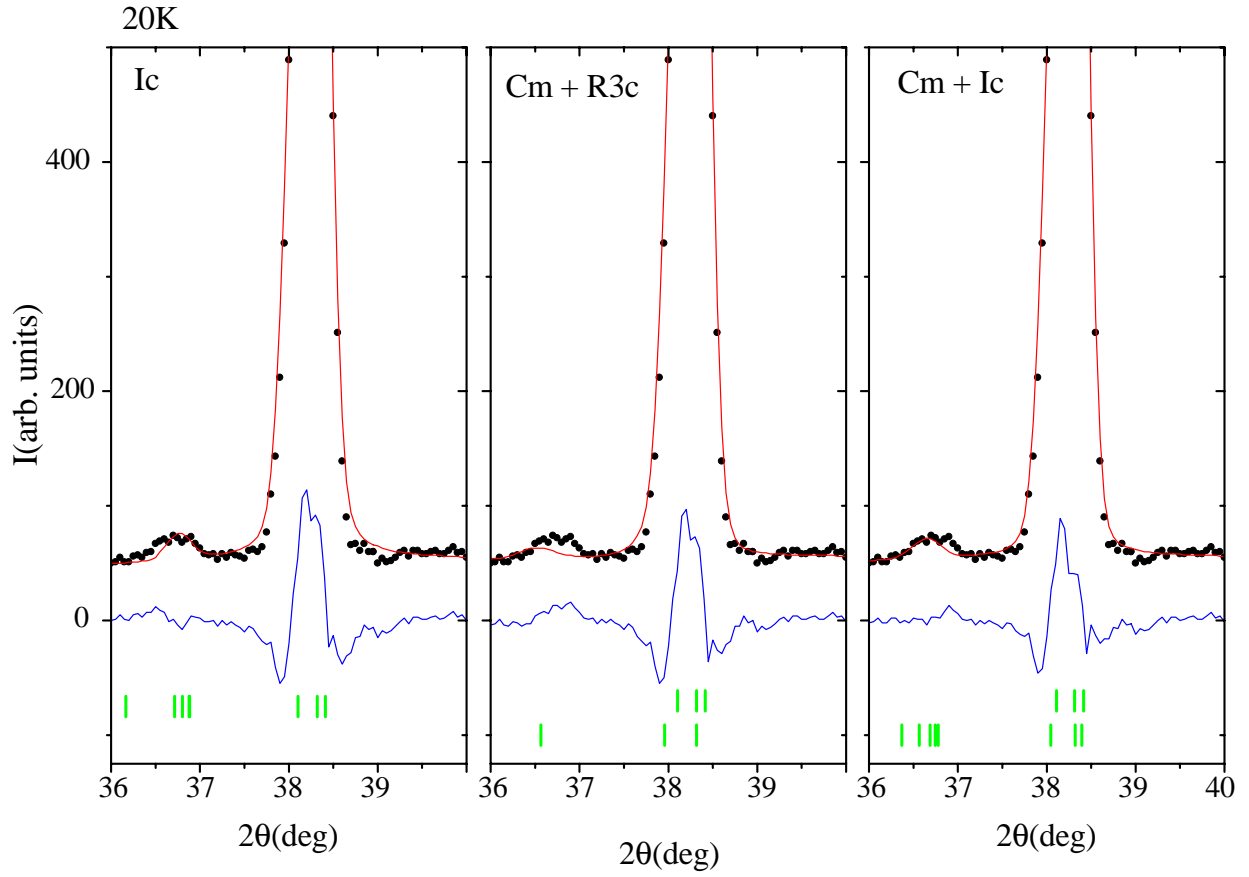


FIG. 4: (Color) Observed and calculated diffraction profiles and difference plots in the region around the strongest superlattice peak from  $\text{PbZr}_{0.52}\text{Ti}_{0.48}\text{O}_3$  at 20 K for single-phase  $Ic$  (left panel), two-phase  $Cm + R3c$  (center panel), and two-phase  $Cm + Ic$  (right panel).

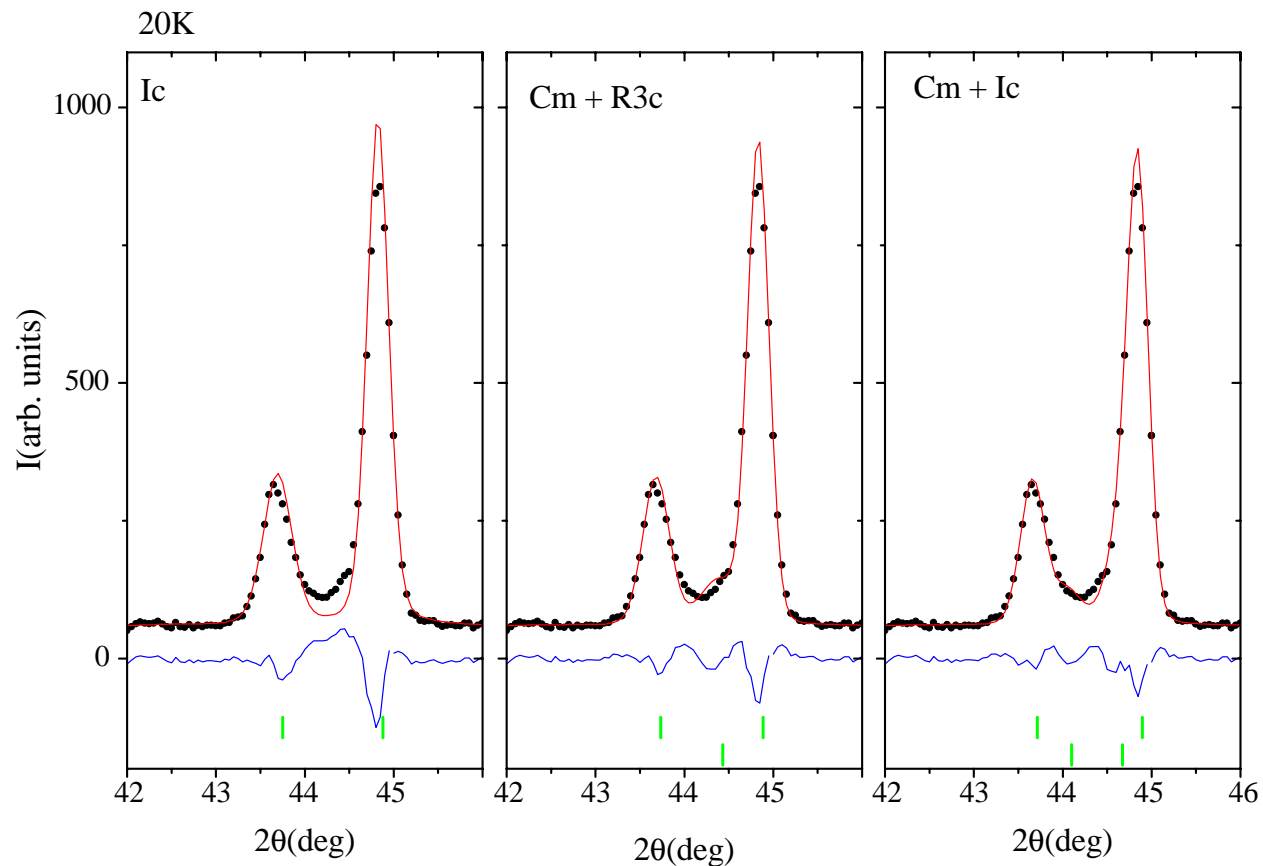


FIG. 5: (Color) Observed and calculated diffraction profiles and difference plots in the region around the pseudocubic (200) reflection from  $\text{PbZr}_{0.52}\text{Ti}_{0.48}\text{O}_3$  at 20 K for single-phase  $Ic$  (left panel), two-phase  $Cm + R3c$  (center panel), and two-phase  $Cm + Ic$  (right panel).

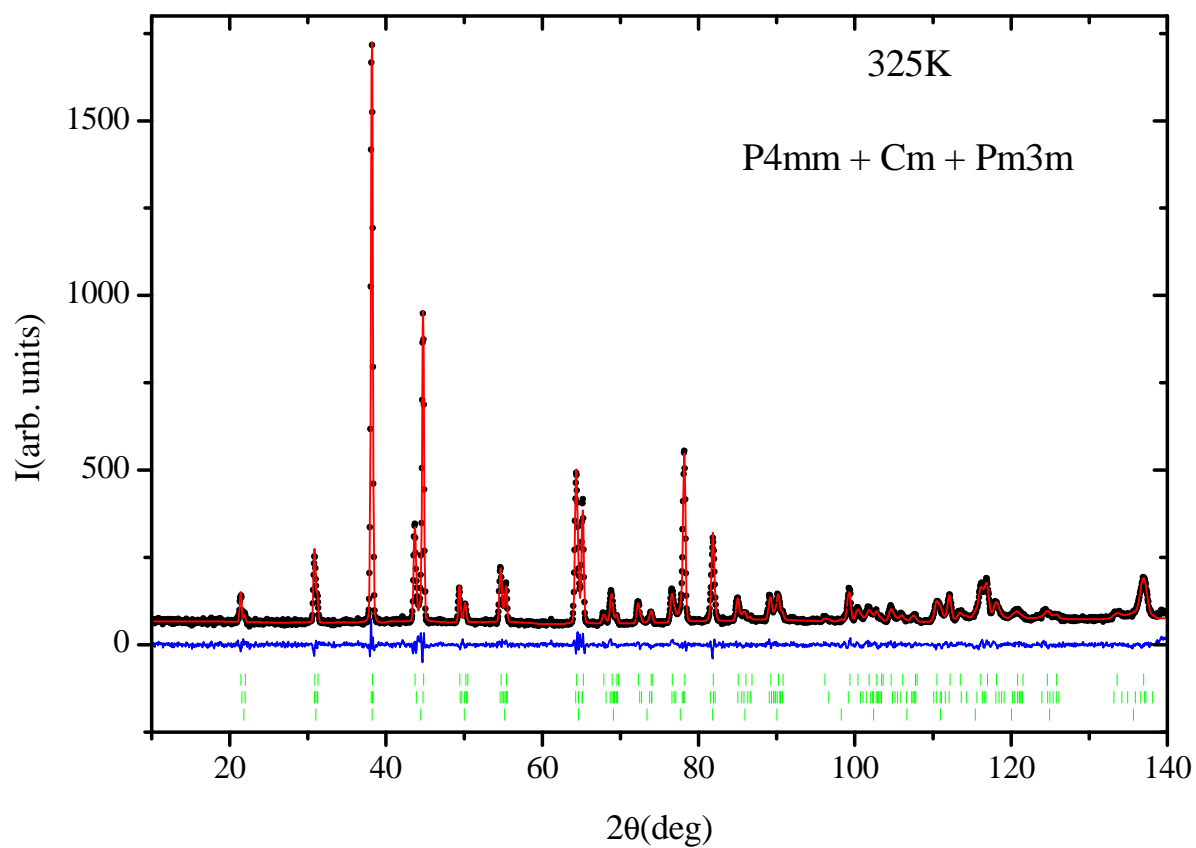


FIG. 6: (Color) Observed and calculated diffraction profiles from the three-phase Rietveld refinement of  $\text{PbZr}_{0.52}\text{Ti}_{0.48}\text{O}_3$  at 325 K, with space groups  $P4mm$ ,  $Cm$  and  $Pm3m$ . The difference plot is shown below, with upper, middle and lower sets of vertical markers denoting the calculated peak positions for  $P4mm$ ,  $Cm$  and  $Pm3m$  respectively.